Stäudle, B., Seynnes, O. R., Laps, G., Göll, F., Brüggemann, G.-P., Albracht, K. (2021). Recovery from Achilles Tendon Repair: A Combination of Postsurgery Outcomes and Insufficient Remodeling of Muscle and Tendon. *Medicine & Science in Sports & Exercise, 53*(7), 1356-1366. http://dx.doi.org/10.1249/MSS.0000000000002592

Recovery from Achilles tendon repair: a combination of postsurgery outcomes and insufficient remodeling of muscle and tendon

Benjamin Stäudle[1;2;3*], Olivier Seynnes[4], Guido Laps[5], Fabian Göll[2], Gert- Peter Brüggemann[3], Kirsten Albracht[1;2]

[1]Faculty of Medical Engineering and Technomathematics, University of Applied Sciences Aachen, Aachen, Germany

[2]Institute of Movement and Neurosciences, German Sport University Cologne, Cologne, Germany

[3]Institute of Biomechanics and Orthopaedics, German Sport University Cologne, Cologne, Germany

[4]Department of Physical Performance, Norwegian School of Sport Sciences, Oslo, Norway

[5]Orthopaedie am Guerzenich, Cologne, Germany

***Corresponding author:**

Benjamin Stäudle

FH Aachen / Campus Jülich

Heinrich-Mußmann-Str.1

52428 Jülich

staeudle@fh-aachen.de

+49 17621239938

Abstract

Introduction: Achilles tendon rupture (ATR) patients have persistent functional deficits in the triceps surae muscle-tendon unit (MTU). The complex remodeling of the MTU accompanying these deficits remains poorly understood. The purpose of the present study was to associate in vivo and in silico data to investigate the relations between changes in MTU properties and strength deficits in ATR patients.

Methods: Eleven male subjects who had undergone surgical repair of complete unilateral ATR were examined 4.6 ± 2.0 (mean ± SD) years after rupture. Gastrocnemius medialis (GM) tendon stiffness, morphology, and muscle architecture were determined using ultrasonography. The force-length relation of the plantar flexor muscles was assessed at five ankle joint angles. In addition, simulations (OpenSim) of the GM MTU force-length properties were performed with various iterations of MTU properties found between the unaffected and the affected side.

Results: The affected side of the patients displayed a longer, larger, and stiffer GM tendon (13 ± 10%, 105 ± 28% and 54 ± 24%, respectively) compared with the unaffected side. The GM muscle fascicles of the affected side were shorter (32 ± 12%) and with greater pennation angles (31 ± 26%). A mean deficit in plantarflexion moment of 31 ± 10% was measured. Simulations indicate that pairing an intact muscle with a longer tendon shifts the optimal angular range of peak force outside physiological angular ranges, whereas the shorter muscle fascicles and tendon stiffening seen in the affected side decrease this shift, albeit incompletely.

Conclusions: These results suggest that the substantial changes in MTU properties found in ATR patients may partly result from compensatory remodeling, although this process appears insufficient to fully restore muscle function.

Key Terms: Tendon rupture; stiffness; simulation; muscle force; muscle fascicle; tendon healing

Abbreviations

ATR	Achilles tendon rupture
CSA	Cross-sectional area
FHL	Flexor hallucis longus
GL	Gastrocnemius lateralis
GM	Gastrocnemius medialis
MTJ	Myotendinous junction
MTU	Muscle-tendon unit

MTU_0	Muscle-tendon unit unaffected side
MTU_1	MTU_0 + longer tendon
MTU_2	MTU_1 + shorter muscle fascicles and greater pennation angle
MTU_3	Muscle-tendon unit affected side
MVCi	Maximal voluntary isometric contraction
PCSA	Physiological cross-sectional area
SEE	Series elastic element

1 Introduction

Achilles tendon rupture (ATR) commonly occurs during recreational physical activity (1). Surgical repair is often prescribed in cases of total rupture, followed by 2 weeks of joint immobilization (2), 6 to 8 weeks wearing an orthotic boot with adjustable ankle angle (3), before starting another 2 to 4 months of active rehabilitation (4). The prognosis is relatively satisfying, with patients being able to resume ambulatory activities and physical activity after 6 months (3, 4). However, side-to-side morphological (5, 6) and functional (7, 8) differences remain in the triceps surae muscle-tendon unit (MTU) several years after surgery. Regardless of treatment strategies (surgical or not), the repaired Achilles tendon becomes longer (8-11), with a long-lasting enlargement of the tendon cross section (12).

From a mechanical point of view, the tendon stiffness of the affected side is lower than in unaffected controls during the first month's post-surgery (13, 14). Observations from animal (14, 15) and human (6, 16) studies suggest that a progressive increase in tendon stiffness takes place during rehabilitation, even exceeding values measured on the unaffected side about 2 years after rupture (17).

Consistent with changes in morphological and mechanical properties of the ruptured Achilles tendon, recent studies have shown concomitant alteration in muscle architecture (9-11, 18). Collectively, these studies indicate a rapid and long-lasting (up to 47 months) decrease in the fascicle length of the gastrocnemius medialis (GM) muscle, while enduring differences in pennation angle have only been observed in one case study, in a patient with poor functional outcome (11).

Tendon mechanical properties and the architecture of a muscle have a profound influence on the contractile behaviour and function of the musculoskeletal system. Tendon deformation conditions the operating length and contraction velocity of muscle fibers, thereby affecting muscle work, force, and efficiency (19, 20). This aspect is particularly interesting in the context of ATR patients, whose strength levels remain lower in the affected side years after surgery (7, 9, 17, 21). Indeed, a longer Achilles tendon may offset the operating range of the triceps surae muscle fibers to shorter lengths (8), although the influence of stiffness recovery and the shortening of muscle fibers on the force deficit of former ATR patients is currently poorly documented.

The purpose of the present study was to undertake a detailed examination of the possible relations between changes in MTU properties and strength deficits in ATR patients. Data were collected

from patients with a history of ATR and surgical repair. We hypothesized that the treated side would present a lower plantarflexion moment within the operating angular range of the healthy side, caused by alterations in MTU properties. Because deficits in force generation are observed years after surgery, we expected muscle fiber shortening and tendon stiffening to mitigate these deficits but to remain insufficient to compensate for the impact of posttreatment tendon lengthening. To support this mechanistic hypothesis, experimental data were used as input variables in simulated isometric contractions of the GM muscle.

2 Methods

2.1 Study design and subjects

Male patients with a history of ATR and surgical repair were recruited for this study. In a cross-sectional design, data were collected in a pseudo randomized order between legs and conditions. The unaffected leg served as control for matched comparisons. Ethical approval was granted by the *institutional review board* of the German Sport University, and all subjects gave written informed consent. Each subject attended two data acquisition sessions separated by a minimum of three days at the Institute of Biomechanics and Orthopaedics of the German Sport University Cologne. The sample size was calculated with the G*Power software (22), based on the deficit in isometric maximal plantar flexion moment at suboptimal MTU length as the primary outcome. This variable was chosen since the main hypothesis of the study is based on strength deficit. Using a mean deficit of 20% and an SD of 19% (23), a β level of 0.8, and an α level of 0.05, the *a priori* power analysis suggested that a minimum sample size of 10 subjects would be necessary.

Because neither time after injury nor initial treatment seem to have an impact on force generation deficits in ATR patients after one year (21), the subjects were chosen to be 2 to 7 years postsurgery and treated with either a modified Bunnel, a Kessler end to end, or with a Dresdner Instrument (minimal invasive) surgery technique. In addition, it was required that the surgery took place within the first 7 days after injury and that subjects' age was in the range of 20 to 60 years. Exclusion criteria consisted of sural nerve injury, tear of the soleus muscle, tendon recurring rupture, and Achilles tendon rupture on the bilateral side. These criteria were obtained by analysing magnetic resonance images and surgery reports with a physician. Cardiovascular complications, self-reported pain in the lower back/ limbs, and other bone/ joint symptoms, precluding the performance of maximal voluntary contractions, were assessed and used as exclusion criteria. Cardiovascular assessment was done using a health questionnaire based on the “Physical Activity

Readiness Questionnaire" (24) recommended by the American College of Sports Medicine. As the purpose of the present study was to undertake a detailed examination of the possible relations between changes in MTU properties and strength deficits in ATR patients, missing data would induce bias. In an effort to reduce the possibility of bias, incomplete datasets (i.e., in cases where subjects did not perform all the required tests) were therefore excluded from the analysis. Patients were recruited from a collaborating medical center (Mediapark Klinik Köln) and by announcements in the local media. Using local media in addition to the medical center was a way to recruit patients with different treatment histories, in an effort to limit recruitment bias.

2.2 Morphology of the triceps surae MTU

Muscle and tendon morphology measurements were based on a previously reported procedure (25) using B-Mode ultrasonography and a 6-cm linear array transducer (Aloka ProSound Alpha-7, Japan, 13 MHz). While subjects were lying prone with the knee and ankle joint in anatomically neutral position (knee fully extended, sole perpendicular to the tibia), the calcaneal insertion and the myotendinous junctions (MTJ) of the gastrocnemii tendon were visualized using ultrasonography and marked on the skin to measure the length of the medial and lateral gastrocnemius (GL) tendons (25). The free Achilles tendon length was measured from panoramic ultrasound scans between the calcaneal insertion and the MTJ of the soleus muscle. This is a modified approach to the validated method of Barfod and colleagues (26), for which a good reliability was demonstrated in healthy subjects. The proximal tendon length of GM and GL (tendon aponeurosis) was calculated as the length difference of the gastrocnemii tendons and the free Achilles tendon. Achilles tendon cross-sectional area (CSA) was measured from transverse plane ultrasound images taken at 25% intervals from the calcaneal insertion to the soleus MTJ. Three images were collected and analyzed (ImageJ, 1.47v, National Institutes of Health) per scanning position and averaged for further analyses. Architecture of the gastrocnemii muscles was assessed from ultrasound scans taken over the mid-muscle bellies (25). The scanning location for the soleus muscle was chosen to optimize fascicle imaging, above the MTJ of the GM muscle. Muscle fascicle length, pennation angle, and muscle thickness were measured offline (Matlab, version R2013b, The Mathworks). The deep and superficial aponeurosis as well as visible parts of three fascicles (i.e., within the field of view) were outlined manually. Pennation angles were defined as the angle between these fascicles and the deep aponeurosis (27). Fascicle length was obtained as the summation of the outlined fascicle sections and nonvisible sections, extrapolated

as straight lines between the edges of the field of view and the aponeuroses (27). Muscle thickness was defined as the perpendicular distance between the deep and superficial aponeuroses in the center of the chosen muscle fascicle (25). Average measurements from three images were calculated for further analysis. All measurements and analysis were performed by the same investigator.

2.3 GM Tendon mechanical properties

After a standardized warm-up, consisting of incremental isometric contractions up to maximum level, three maximal isometric plantarflexions were performed to determine maximum force. The mechanical properties of the GM tendon, consisting of the free Achilles tendon and the tendinous tissue between the GM MTJ and the soleus MTJ, was then examined by measuring GM tendon elongation during 5- second isometric ramp contractions up to 80% of maximum effort (28). Visual feedback was provided to ensure a linear increase in force. The stiffness of the GM tendon was measured as a surrogate of Achilles tendon stiffness. This measure was chosen because it involves the main structures of the Achilles tendon and because of the current difficulty to test the stiffness of the whole Achilles tendon in vivo (29).

Subjects were seated in a custom-made dynamometer with their foot firmly strapped to a force plate with their ankle and knee joints at 0° (knee fully extended, sole perpendicular to the tibia) and their hip joint flexed at 70°. To determine GM tendon elongation, the linear array ultrasound transducer (Aloka ProSound Alpha-7, Japan, 13 MHz, 73 Hz frame rate) was attached longitudinally over the GM MTJ (13, 17, 25), using a custom-made case and elastic bandages. The point of force application and the vertical reaction force were assessed by three one-dimensional strain gauge force sensors embedded under the footplate. Reflective markers were positioned on anatomic landmarks of the subject's leg (medial and lateral calcaneus, 2nd metatarsal joint, malleolus lateralis, malleolus medialis, tibial tuberosity), force plate, and ultrasound transducer (Fig. 1). The magnitude of the external ankle joint moment was calculated from the perpendicular reaction force and the vector connecting the ankle joint center (midpoint of both malleoli markers) and the point of force application. The resulting joint moment was corrected for antagonistic co-activation of the tibialis anterior muscle (30). Forces acting parallel to the footplate as well as the weight of the foot were neglected.

Achilles tendon force was calculated by dividing the resulting joint moment by the Achilles tendon moment arm, estimated with the tendon excursion method (31, 32). A three-dimensional motion

capture system (Vicon Nexus, Oxford, UK) was used to simultaneously acquire marker trajectories (100 Hz) and analog signals (1 kHz). The ultrasound system was time synchronized by sending a rectangular impulse through the electrocardiography channel.

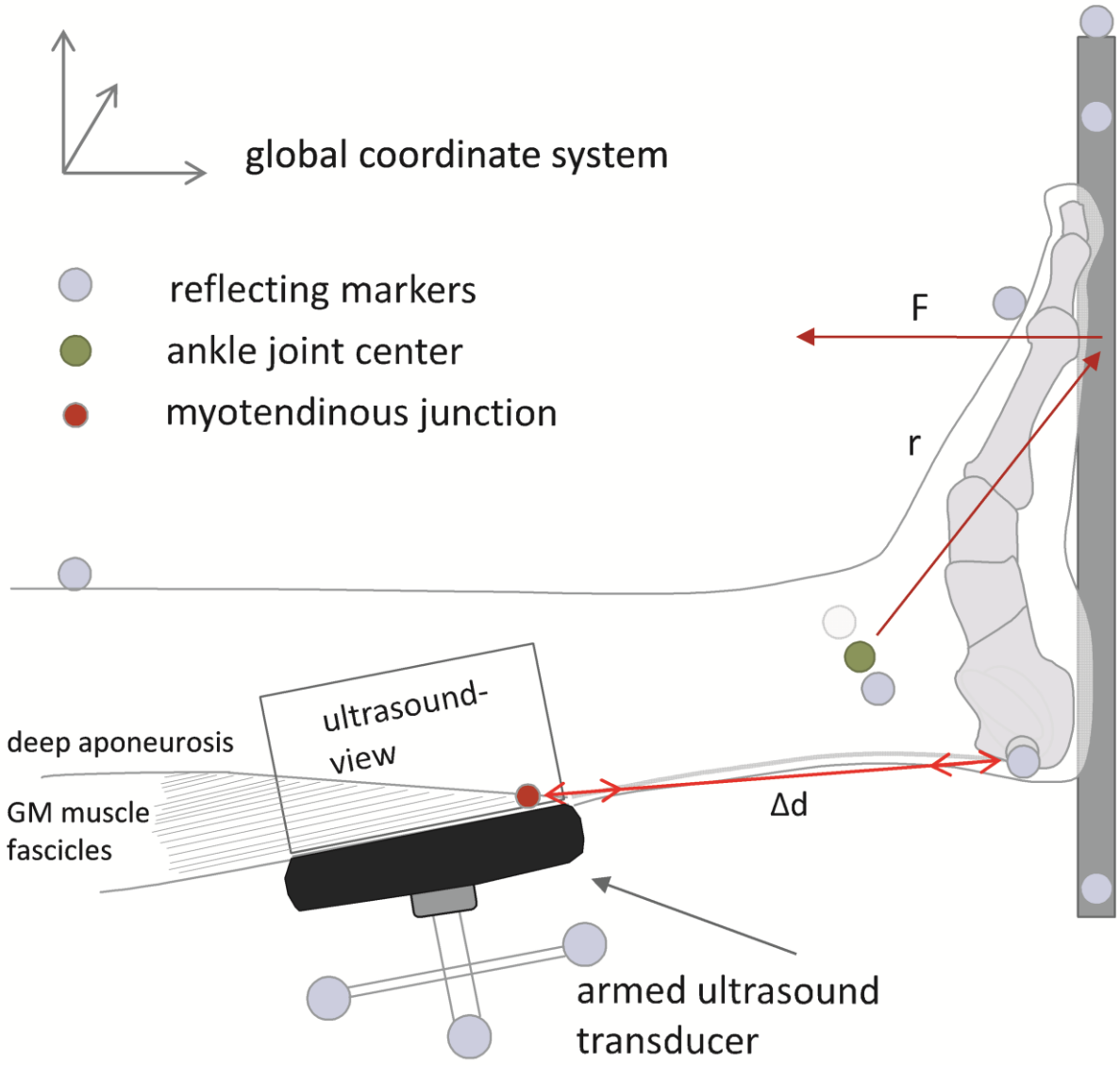

FIGURE 1. Experimental set-up used to quantify tendon mechanical properties. F: vertical reaction force, r: vector connecting ankle joint centre and point of force application, Δd: distance between the myotendinous junction (red dot) and the osteotendinous insertion represented by the projection midpoint of the medial and lateral calcaneus marker.

The displacement of a muscle fascicle intersection point with the deep aponeurosis close to the GM MTJ was analyzed in the 2D ultrasound image with a semi-automatic tracking software (Tracker 4.84, physlets.org/tracker/) (33). The three markers attached to the ultrasound transducer

enabled the transformation of that point into the global reference system. Tendon length changes were then defined as a change in the distance between the fascicle intersection point and the osteotendinous insertion represented by the midpoint of the medial and lateral calcaneus marker on the skin (34)(Fig. 1). Each tendon force-elongation relationship was temporarily fitted with a second-order polynomial without a constant term to exclude trials with a coefficient of determination lower than 0.9 from further analysis (33). The remaining trials for each leg were averaged and fitted with a second-order polynomial without a constant term.

To compare the affected and unaffected side on a common tendon force level, GM tendon stiffness was calculated in the force interval between 60 and 80% of the maximum isometric contraction (MVCi) of the affected side. Young's modulus, was calculated by multiplying the GM stiffness with the fraction of GM tendon resting length and average tendon CSA. At a force level corresponding to 80% MVCi of the affected side, tendon stress was calculated as the quotient of tendon force and mean CSA and GM tendon strain as the percentage of tendon elongation relative to resting length. In addition, GM tendon strain at 80% MVCi of the unaffected side was determined to obtain appropriate values to scale the serial elastic element (SEE) of the muscle-tendon model.

2.4 Moment-angle relationship

A custom-made dynamometer was used to determine the moment-angle relationship of the plantarflexor muscles (35). Subjects were seated in an upright position with the hip and knee joints flexed at 90°. The joint center of the ankle joint was carefully aligned with the axis of rotation of the dynamometer. A strain gauge force sensor was embedded under the foot platform. Ankle joint moment was determined by multiplying the measured force with the external moment arm, the perpendicular distance between the force sensor and axis of rotation. A figure of the dynamometer can be found in the Supplemental Digital Content 1 (see Figure, Supplemental Digital Content 1, http://links.lww.com/MSS/C242).

After a standardized warm-up consisting of incremental isometric contractions up to maximum level, subjects performed a series of maximal isometric contractions at ankle joint angles of -20,-10, 0, 10 and 20°, with 0° representing the neutral position, and positive angles indicating plantarflexed positions. The trial with the highest moment for each tested angle was taken for further analyses. Ultrasound scanning of the GM enabled acquiring images of muscle architecture during the maximal isometric contraction. To assess the inevitable movement of the knee and ankle

joint during the contractions (36, 37), trajectories of reflective markers attached to the trochanter major, lateral femur condyle, lateral malleolus, and fifth metatarsal phalangeal joint were recorded with a motion capture system with 5 Vicon MX40 infrared cameras and a frame rate of 100 Hz (Vicon, Oxford, UK). Using kinematics information, maximum joint moments from the affected side were linearly interpolated at the ankle joint positions at which maximum joint moments were generated on the unaffected side.

2.5 Statistical analysis

D'Agostino and Pearson normality test were applied to check whether the data were normally distributed. A two-way repeated-measure ANOVA (side and joint angle as main effects) was used to identify interactions between the affected/unaffected sides and the moment-angle relationship. For all other parameters dependent-sample *t*-tests or Wilcoxon signed rank tests were used to identify differences between sides. All tests were performed in GraphPad Prism (v 7.02) with a significance level of $\alpha = 0.05$. Values are reported as means ± SD in text and means ± SEM in the figures.

2.6 Computer simulations

Isometric contractions of the GM muscle were simulated with a modified "gait10dof18musc" musculoskeletal model in OpenSim 4.0 (38, 39). The modified model consists of six rigid bodies (femur, tibia, fibula, talus, calcaneus, and toes) and a model of the GM MTU (40). The length of the tibia segment was scaled to the average shank length of the subjects (429 mm), determined as the distance from the lateral edge of the tibial plateau to the lateral malleolus. The foot segments (talus, calcaneus, and toes) were scaled to match the average Achilles tendon moment arm of the subject's unaffected side (45 mm). To scale the generic muscle-tendon model, optimal muscle fiber length, pennation angle at optimal muscle fiber length, maximum isometric force, slack length of the SEE, and strain of SEE at maximum isometric force were adjusted to reflect average muscle and SEE properties of the affected and unaffected sides.

For optimal muscle fiber length and pennation angle at optimal muscle fiber length, the average fascicle length and pennation angle were obtained from ultrasound scans performed at rest, in the anatomical neutral position. Slack length of the SEE was calculated as the difference between the MTU length and the projected optimal muscle fiber length. Strain of the serial elastic element (SEE) at maximum isometric force was determined by extrapolating the experimentally determined strain at 80% MVCi. The maximum isometric force of the GM muscle was estimated

by multiplying the Achilles tendon force at MVCi of the unaffected side with the relative fraction of the muscle physiological CSA of cadaveric specimen (25.5% of the triceps surae muscle) (41). To better apprehend the functional implications of the GM tendon and muscle properties measured in the affected leg, simulations were performed for four different MTU configurations, with variations in tendon length, muscle architecture and tendon stiffness. These different MTU configurations and their muscle-tendon specific scaling factors are listed in Table 1.

TABLE 1. Muscle-tendon specific parameters used to scale the generic muscle-tendon model.

	$F_0^{CE}[N]$	L_0^{CE} [mm]	α_0^{CE} [°]	$\bar{L}_S^{SEE}$ [mm]	ε_0^{SEE}[%]
MTU_0	1357	63	19	390	4.9
MTU_1	1357	63	19	416	4.9
MTU_2	1357	42	24	416	4.9
MTU_3	1357	42	24	416	2.9

F_0^{CE}: maximum isometric muscle force, L_0^{CE} : optimal muscle fiber length, α_0^{CE} : muscle fiber pennation angle at optimum muscle fiber length, $\bar{L}_S^{SEE}$: slack length of series elastic element (SEE), ε_0^{SEE} : strain of SEE at maximum isometric force. MTU_0 represents the muscle-tendon unit of the unaffected side. MTU_1 has the same properties as MTU_0 but a longer tendon. MTU_2 has the same properties as MTU_1 but shorter fascicles and greater pennation angles. MTU_3 has the same properties as MTU_2 but a stiffer tendon and thus represents the muscle-tendon unit of the affected side.

Assuming full muscle activation, active muscle force was computed as a function of ankle joint angle. Simulations were done in two different knee joint configurations (extended/ 90° flexed) with a range of ankle joint angles from 60° plantarflexion to 60° dorsiflexion.

3 Results

Eleven out of the 14 subjects recruited for the trial completed all sets of measurement and were included in the final analysis (Fig. 2). The baseline characteristics of these subjects are reported in Table 2.

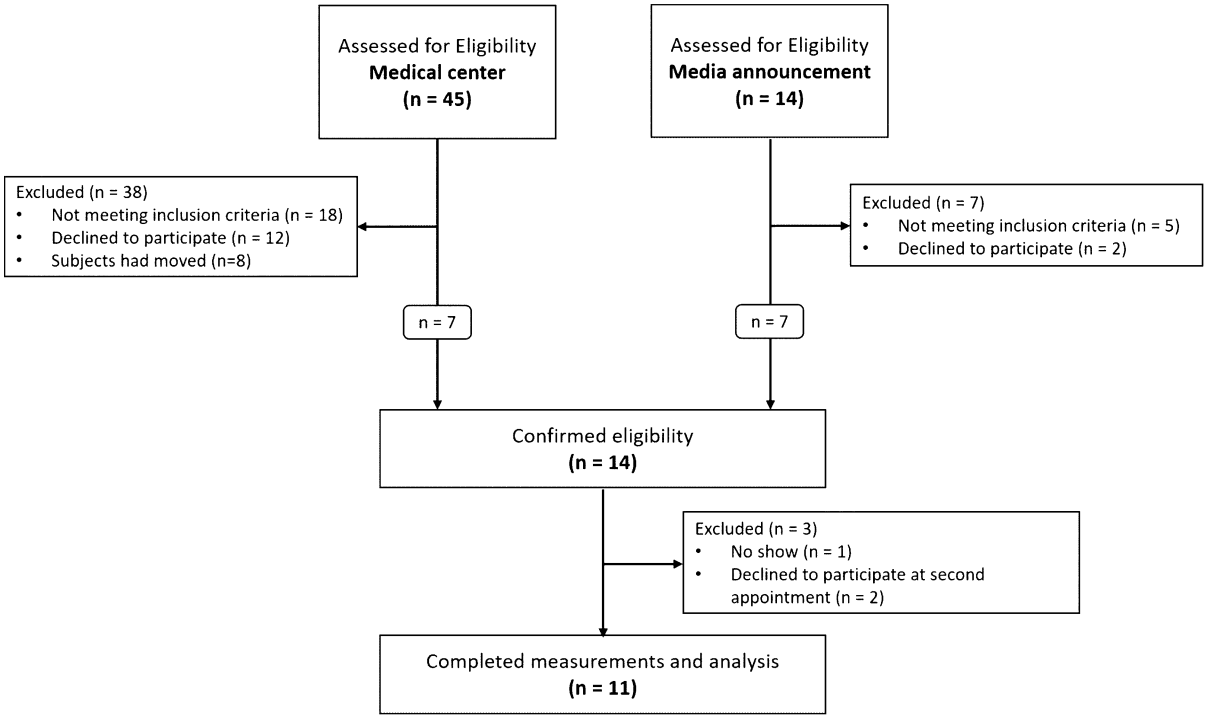

FIGURE 2. Flow chart illustrating the recruitment and inclusion of subjects at each stage of the trial.

TABLE 2. Subjects demographic characteristics in mean ± SD.

Sample size	Age [yrs.]	Height [cm]	Mass [kg]	Time post-surgery [yrs.]	Time to surgery [days]
11	44.1 ± 11.3	179 ± 8	79.5 ± 10.6	4.6 ± 2	3.5 ± 1.7

3.1 Muscle tendon morphology

The parameters describing tendon and muscle morphology are summarized in Table 3. Free Achilles tendon length was significantly longer (22 ± 22 mm) on the affected side, but no significant differences were observed in the length of the proximal part of the gastrocnemii tendon. Achilles tendon CSA was significantly greater in all regions of the affected tendon (Table 3). On average, tendon CSA was 105 ± 28% larger. In addition, Achilles tendon moment arm was significantly shorter (14% ± 10%) on the affected side.

Muscle thickness was significantly smaller in the GM (12 ± 12%) and GL (10 ± 12%) muscles of the affected side compared to the unaffected side, but not in the soleus muscle. Other architectural parameters of the triceps surae muscles were significantly different between sides. In the affected side, fascicle length was 32 ± 12%, 27 ± 14%, and 34 ± 18% shorter in the GM, GL and soleus

muscles, respectively, whereas pennation angle was 31 ± 26%, 25 ± 31%, and 45 ± 44% larger, respectively.

TABLE 3. Parameters describing tendon and muscle morphology assessed in neutral position of the ankle and knee joint.

	Affected leg	Unaffected leg			
Tendon parameters	mean ± SD	mean ± SD	differences	95% CI	p-value
Free AT l_T [mm]	82 ± 22	61 ± 17	22 ± 22	7 to 37	0.009
Proximal GM l_T [mm]	143 ± 23	139 ± 24	4 ± 34	-19 to 26	0.721
Proximal GL l_T [mm]	162 ± 24	165 ± 28	-3 ± 25	-20 to 14	0.709
CSA 0% [mm^2]	112 ± 51	80 ± 19	32 ± 45	0 to 64	0.019
CSA 25% [mm^2]	155 ± 43	87 ± 14	68 ± 40	41 to 95	<0.001
CSA 50% [mm^2]	179 ± 50	77 ± 18	102 ± 40	75 to 129	0.001
CSA 75% [mm^2]	177 ± 20	72 ± 12	105 ± 23	90 to 120	<0.001
CSA 100% [mm^2]	168 ± 34	75 ± 18	93 ± 36	68 to 119	<0.001
Tendon MA [mm]	38 ± 4	45 ± 4	-6 ± 5	3 to 9.4	0.001
Muscle parameters					
GM thickness (mm)	16.3 ± 3	18.4 ± 1.6	-2.2 ± 2.2	-3.7 to -0.7	0.008
GL thickness (mm)	13.6 ± 2	15.3 ± 2.8	-1.7 ± 2.2	-3.2 to -0.2	0.030
SOL thickness (mm)	14 ± 2	16.1 ± 3.1	-2.1 ± 3.1	-4 to 0	0.054
GM l_F (mm)	42 ± 6	63 ± 6	-21 ± 9	-27 to -15	<0.001
GL l_F (mm)	56 ± 14	77 ± 12	-21 ± 12	-29 to -13	<0.001
SOL l_F (mm)	30 ± 6	47 ± 5	-16 ± 9	-23 to -10	<0.001
GM Φ (°)	24.3 ± 3.3	18.9 ± 2.8	5.4 ± 3.6	3 to 7.8	<0.001
GL Φ (°)	15.5 ± 2.6	12.6 ± 2.3	2.8 ± 2.8	1 to 4.7	0.007
SOL Φ (°)	28.7 ± 5.4	20.6 ± 3.8	8.1 ± 7.3	3.2 to 13	0.004

Values are presented as mean ± SD. CI: confidence interval, free AT l_T: Achilles tendon length, proximal GM l_T: length of the gastrocnemius medialis aponeurosis, proximal GL l_T: length of the gastrocnemius lateralis aponeurosis, CSA: cross-sectional area, MA: moment arm, GM: gastrocnemius medialis muscle, GL: gastrocnemius lateralis muscle, SOL: soleus muscle, l_F: fascicle length, Φ: pennation angle.

3.2 GM Tendon mechanical properties

Figures 3A and B show the differences in GM tendon properties of the affected compared to the unaffected side. GM tendon stiffness was 54 ± 24% higher in affected tendons (1160 ± 222 $N \cdot mm^{-1}$ vs. 755 ± 108 $N \cdot mm^{-1}$; $p < 0.001$), whereas tendon stress (22.3 ± 3.7 MPa vs. 43.1 ± 8.2 MPa, $p < 0.001$) and tendon strain (2.48 ± 0.65% vs. 3.9 ± 0.5%, $p = 0.001$) were significantly smaller with differences of 47 ± 9% and 37 ± 11%, respectively. GM tendon strain at MVCi of the

unaffected side, used to scale the SEE of the generic muscle model, was also significantly smaller (41 ± 11%) in the affected side (2.9 ± 0.8% vs. 4.9 ± 0.7%, p = 0.001). Young's modulus did not differ between sides (1692 ± 515 N/mm^2 vs. 1866 ± 433 N/mm^2, p = 0.152). Percentage differences between legs are displayed in Figure 3B.

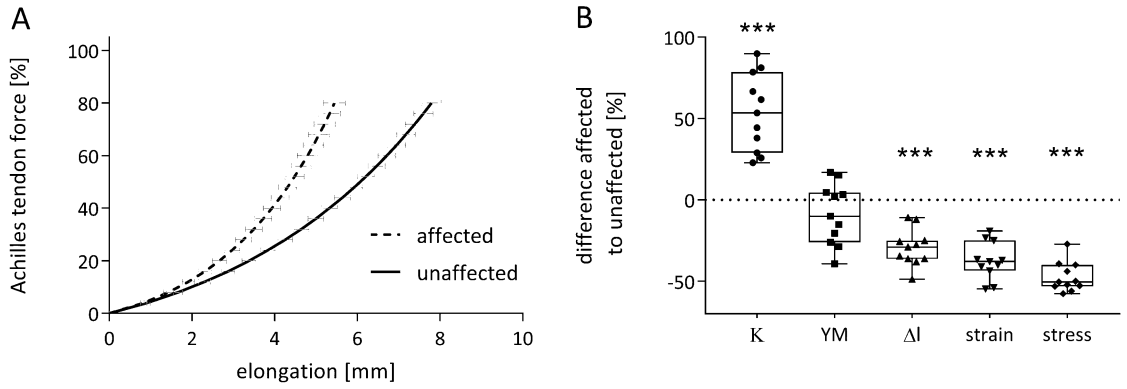

FIGURE 3A. Achilles tendon force-deformation relation for the affected (dashed line) and unaffected (solid line) side. Achilles tendon force (ATF) is expressed relative to the maximum of the affected side for each individual subject (80% of maximum ATF = 3503 ± 518 N). (B) Boxplots of relative differences between the affected and unaffected side, representing minimum, 25th percentile, median, 75th percentile and maximum. Significant difference between sides: *p < 0.05, **p < 0.01, ***p < 0.001. K: tendon stiffness, YM: Young's modulus, Δl: tendon elongation.

3.3 Moment-angle relationship

The plantarflexion moment-ankle joint angle relationship and the corresponding results for fascicle length and pennation angle of the GM muscle are shown in Figure 4. The plantar flexion moment and fascicle length were significantly lower in the affected leg, with mean differences from control of 31 ± 10% and 23 ± 6%, respectively. Pennation angle was significantly greater in the affected muscle, with a mean difference of 28 ± 17%. The maximum moment was significantly lower (133 ± 36 Nm vs. 158 ± 38 Nm, p = 0.007) on the affected side compared to the unaffected side and occurred at a significantly more dorsiflexed joint angle (-7.2 ± 4° vs. 1.6 ± 3.7°, p < 0.001), whereas GM fascicles were significantly shorter (18 ± 3 mm vs. 22 ± 3 mm, p < 0.001) and pennation angles larger (65 ± 7° vs. 54 ± 7°, p = 0.002) on the affected side.

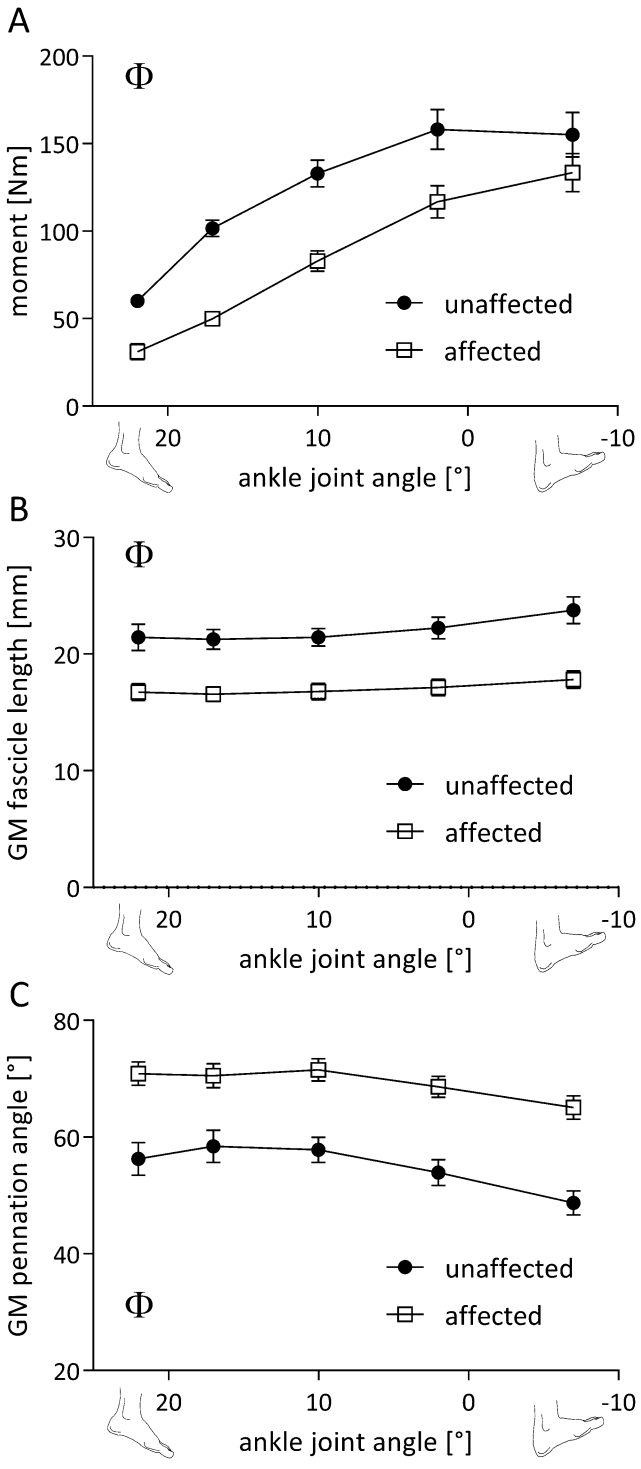

FIGURE 4. The plantarflexion moment-ankle joint angle relationship (A) and the corresponding results for fascicle length (B) and pennation angle (C) for the gastrocnemius medialis muscle (GM) during maximum isometric contraction. Φ: significant leg effect ($p < 0.001$). Positive values on the x-axis represent plantarflexion, negative values dorsalflexion.

3.4 Computer simulations

Figures 5A and B show the active GM muscle force for different MTU properties, as a function of ankle joint angle, with the knee extended or flexed, respectively.

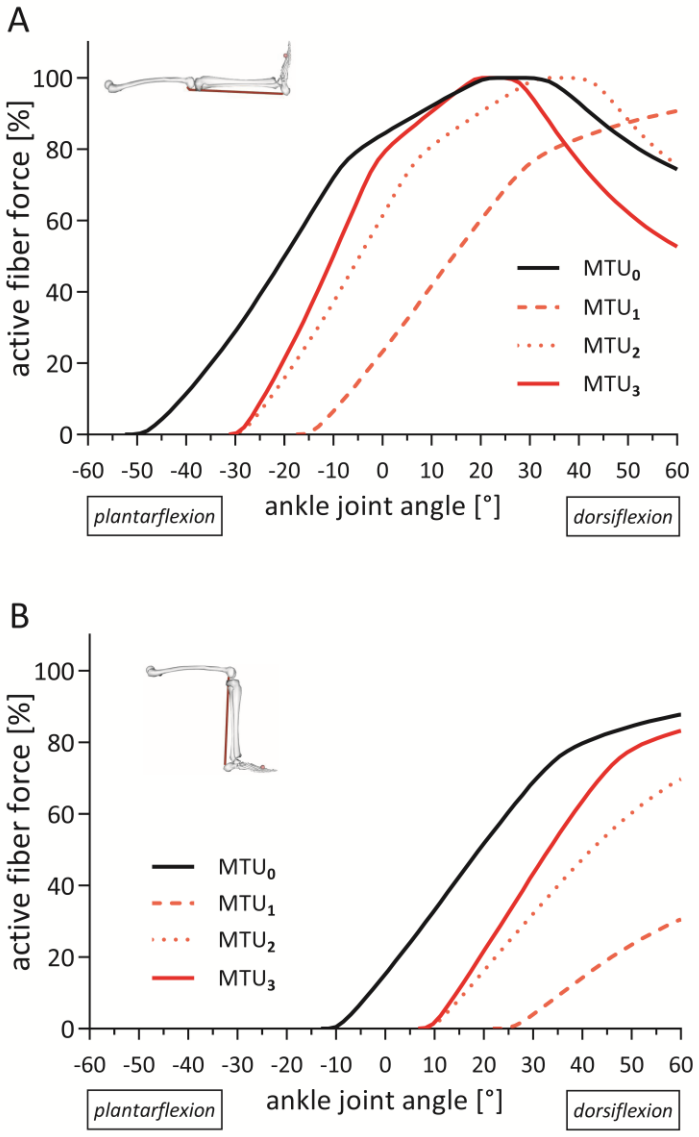

FIGURE 5. Active gastrocnemius medialis fiber force in relation to ankle joint angle with an extended knee (A) and a 90° flexed knee (B). MTU_0 represents the muscle-tendon unit (MTU) of the unaffected side. MTU_1 has the same properties as MTU_0 but a longer tendon. MTU_2 has the same properties as MTU_1 but shorter fascicles and greater pennation angles. MTU_3 has the same properties as MTU_2 but a stiffer tendon and thus represents the MTU of the affected side.

The MTU representing the unaffected side (MTU_0) reaches the active fiber force plateau with the knee fully extended and the ankle joint angle ranging from 22° to 32° dorsiflexion (Fig. 5A). With

a longer tendon modelled to the architectural features of MTU_0, represented by MTU_1, peak active fiber force could not be reached within the simulated range of dorsiflexion (60°). The minimum ankle joint angle at which force can be generated then shifts from 49° to 16° of plantarflexion when the knee is extended (Fig. 5A) and from 12° of plantarflexion to 25° of dorsiflexion when the knee is flexed at 90˚ (Fig. 5B).

When a longer tendon is coupled with shorter fascicles and a greater pennation angle (MTU_2), a shift in the optimal angle for active fiber force is still observed but less pronounced than in MTU_1 (Fig. 5A). The force plateau in MTU_2 is presented by ankle joint angles ranging from 32 to 40° of dorsiflexion. The minimum ankle joint angle to generate force shifts to 30° of plantarflexion.

When tendon stiffness is increased with a configuration corresponding to MTU_2 (MTU_3), the model reflects more closely the properties measured in the affected side. Under these conditions, the peak active fiber force is achieved at ankle joint angles ranging from 19° to 26° of dorsiflexion, similar to the "unaffected" model, MTU_0 (Fig. 5A). The ankle angular range over which the force plateau is achieved is, however, slightly reduced in MTU_2 and MTU_3 compared to MTU_0 when dorsiflexion increases (Fig. 5A). The minimum ankle joint angle to generate force remains at 30° of plantarflexion, which also corresponds to an ankle joint angle of 8° dorsiflexion with a flexed knee.

When quantifying maximal force generating capacity at a neutral ankle joint angle and extended knee joint, deficits of 71% (MTU_1), 26% (MTU_2) and 6% (MTU_3) are observed relative to MTU_0 (100%). Deficits become even larger with a flexed knee and 20° of ankle dorsiflexion, reaching deficits of 100% (MTU_1), 68% (MTU_2), and 57% (MTU_3).

4 Discussion

The aim of the present study was to get a better understanding of the strength deficit of the triceps surae muscle-tendon complex observed 2 to 7 years following complete ATR postsurgery. Our findings confirmed previous reports indicating elongated and stiffer GM tendons as well as a decrease in fascicle length in patients with history of ATR, suggesting an architectural re-organisation of the triceps surae MTU. Consistent with our hypothesis, these changes were accompanied by a shift in the optimal ankle joint angle of moment production towards more dorsiflexed positions. Taken together, the experimental data suggest that the deficits in force generation seen in ATR patients may be mitigated by shorter muscle fascicles and a stiffer GM tendon but remain insufficient to compensate all the adverse effects of posttreatment lengthening.

Computer simulations suggest that the architectural reorganisation and tendon stiffening observed in ATR patients may help restoring prerupture capacity of maximal force production, whereas these changes remain ineffective to prevent a loss of force at shorter MTU lengths.

4.1 Strength deficit

Large strength deficits of the plantar flexor muscles could be observed in the investigated ATR patients. The average plantarflexion strength deficit observed in the affected side amounts to 31% and is in line with recent observations from ATR patients with functional impairment (9). The current strength deficits may partly be attributable to the 12 % and 10 % smaller muscle thickness measured in GM and GL, respectively. Nonetheless, such a difference in muscle size cannot entirely account for the largest strength deficits (up to 48%) seen at certain joint angles. This discrepancy suggests that other factors than muscle atrophy affect the force deficit over the entire operating range of the plantar flexor muscles. The fact that the affected side exerts a maximum moment at a significantly more dorsiflexed ankle joint angle than the unaffected side supports this assertion and the hypothesis of changes in the triceps surae force-length relation.

4.2 GM tendon properties

The biomechanical and morphological characteristics observed in the repaired GM tendon are obvious candidates to explain differences in the force-length relationship. In the current study, the surgically treated GM tendons were 26 mm longer than the GM tendon on the unaffected side, which is consistent with the literature reporting differences in tendon resting length ranging 15 to 27 mm more than one year after surgery (8, 9, 17). The present results show that lengthening occurred mainly in the so-called free portion of the Achilles tendon. Despite being longer, affected GM tendons were stiffer (54 ± 24%) than unaffected ones, although similar Young's modulus values suggest for the first time that the material properties of the affected tendon may be restored to values similar to the unaffected side, 4.6 years postsurgery. The higher stiffness of repaired GM tendons seems thus mainly attributable to the considerable differences in tendon CSA (105 ± 28%). From a functional perspective, a greater tendon stiffness limits deformation at a given load and would mitigate the excessive strain expected in the longer affected tendon. This trade-off arguably helps preserving favorable contractile conditions for the triceps surae muscles, by limiting excessive shortening of muscle fibers.

4.3 Architecture

Despite the positive influence of tendon stiffening postulated above, we found substantial architectural remodeling of the triceps surae muscles, with 27-to-34% shorter fascicles and 25-to-45% larger pennation angles in the affected side. These observations confirm very recent findings of shorter fascicles in the GM muscle of ATR patients (9-11) and are in agreement with one study reporting an increase in pennation angle (11). The magnitude of affected-to-healthy architectural differences differs considerably between studies (17-59% for fascicle length and no significant difference to 162% for pennation angle). This disparity is expectable, owing to the differences in patient background, injury profile, duration post-surgery, and in methodology.

Muscle architectural remodelling is typically ascribed to adaptive addition or removal of sarcomeres as shown in animal studies (42, 43), immobilizing limbs in stretched or shortened positions, respectively. The ability of muscle to sense mechanical signals (change in tension) to regulate protein turnover in humans has been shown consistently and is often linked to architectural reorganisation (44-46).

4.4 Computer simulations

The computer simulations confirmed our hypothesis of a detrimental effect of tendon elongation on GM's force generation ability, which may partly be compensated for by changes in muscle architecture and tendon stiffening.

All things being equal, the model showed that a 26 mm longer GM tendon causes a shift in the operating range of fascicles towards longer MTU length, whereby peak forces could not be generated at functional joint configurations (i.e., ankle joint angle until 60° dorsiflexion; see MTU_1 in Fig. 5A). Such a shift would result in a 28% reduction of contractile force in comparison to the maximum force plateau of the unaffected side (MTU_0 in Fig. 5).This is in agreement with the 23% reduction in contractile force predicted for a 2 cm tendon lengthening in other *in silico* data (47).

To what extent would architectural differences observed in ATR patients, had they represented true sarcomeric remodelling, mitigate the negative impact of tendon lengthening? The simulations demonstrate that comparable shortening of muscle fibers and increase in pennation angle (MTU_2 in Fig. 5A) is sufficient to shift the muscle's operating range and the optimal angular range for peak force back and thus closer to physiological values. Interestingly, when observing experimental data and simulations of the flexed knee condition (Fig. 5B), representing shorter MTU lengths, the gastrocnemii muscles of the affected side do not even contribute to force

generation in the experimental range of ankle joint angles (22° plantarflexion to 7° dorsiflexion). Taken together, these data support our assumption that the removal of in series sarcomeres resets sarcomere optimal operating length to original values. However, such a reduction of in series sarcomeres also restricts the active operating range of muscle fibers, resulting in a force deficit at shorter MTU lengths. Therefore, the influence of muscle atrophy seems less important to explain the present findings than the changes discussed above.

A stiffening of the GM tendon was expected to have similar effects on the force-length relationship as the reduction in serial sarcomeres, albeit to a lower extent. Nonetheless, when added to the MTU model (MTU_2) with altered tendon length and muscle architecture to fully mimic our findings in ATR patients (MTU_3 in Fig. 5), the stiffer tendon enabled the muscle peak active force to occur at even shorter MTU lengths than in the unaffected side (MTU_0). Therefore, as pointed out previously (47), the stiffer tendon in MTU_3 shifts the optimal MTU length and ankle angle to control values by steepening the slope of the force-length curve and thereby being ineffective against force deficits outside optimal ranges.

Finally, the differences in moment arms observed between affected and healthy sides in these patients likely influence the moment-angle relation (48). We tested this hypothesis by modelling the affected muscle tendon unit with all the characteristics measured in the present study, with a corresponding moment arm length (38mm) and with a moment arm length of the unaffected side (45mm). The result shows that, with a fully extended knee, the smaller moment arm of the affected MTU has a marginal effect on maximal active force production. Clearer, yet functionally less important effects can be seen as about 10% differences in force production at nonphysiological dorsiflexion angles. For the sake of clarity, we include the modelled differences in moment arm in a separate figure in the Supplemental Digital Content 2 (see Figure, Supplemental Digital Content 2, http://links.lww.com/MSS/C243).

4.5 Limitations

The *in silico* study of the influence of MTU properties on limb function offers a powerful tool that is not devoid of limitation. Muscle modelling cannot entirely reflect *in vivo* conditions due to a number of limitations. For instance, we could not model the force-length relation of the subjects individually, nor could we implement all possible variables describing muscle properties. Nonetheless, using the means as input variables and keeping other parameters fixed to standard values throughout all conditions and between sides was allegedly sufficient here. With the aim to

demonstrate the influence of substantial changes measured in the MTU of tendon rupture patients, our model would not have yielded different conclusions with a greater level of accuracy. In addition, the present study only included a model for the GM muscle. Despite being a relatively important plantar flexor, this muscle contributes far less than the monoarticular soleus muscle. Future investigations may complete the present findings with an analysis based on the soleus muscle.

This study focused on the mechanical and morphological features affecting force generation and the impact of other parameters – not measured here – cannot be predicted. A reduction in neural drive caused by cortico-motor inhibition may also affect force generation after injury. To the best of our knowledge, information on the contribution of neural drive to strength deficits in ATR patients is thus far lacking and is warranted to complement the present results.

Another methodological consideration should be made regarding the assessment of tendon force and mechanical properties. Our method is based on the assumption that the triceps surae force explains nearly all the plantarflexion moment, neglecting the possible hypertrophy of synergist muscles previously observed in ATR patients (e.g., 5% flexor hallucis longus) (49). Such a hypertrophy could lead to an overestimation of tendon force and stiffness on the affected side. However, based on previous reports, the 7.7 cm^3 hypertrophy of the flexor hallucis longus and deep flexors account less than 1% to the total volume of all plantar flexor muscles (1031 cm^3) (49). Therefore, we believe the hypertrophy of synergist muscles to have a negligible impact on force distribution within the plantar flexor muscles several years after ATR.

Finally, caution should be exercised when inferring the present findings to female patients. The choice of recruiting male participants only was made in an attempt to preserve statistical power, by avoiding the variability in tendon properties inherent to hormonal influences in a female population (50). Additional research is warranted to ascertain the present results with a larger sample of ATR patients including females.

4.6 Clinical perspective

The results based on our model illustrates the extent of functional deficits stemming from tendon lengthening in ATR patients. They also reflect how alterations in fascicle length and tendon stiffness may not entirely counteract these deficits, as seen with a narrower torque-angle relation in the affected side. Functional limitations may therefore occur in activities requiring large angular excursions of the ankle joint (e.g., unilateral heel-rises, jump landings, stair descent, and certain

locomotor tasks). Unfortunately, this analysis alone does not offer further information on clinical outcomes, nor can it predict the long-term effect that a reduced or corrected (revision surgery) tendon lengthening would have. The latter merits consideration.

Simple trigonometric calculations suggests that alterations in muscle architecture (shortening of muscle and fibres) may have compensated the increased tendon slack by 80% (21mm), although lesser tendon slack was fully accounted for by architectural alterations in one other study (10). In the same line of thought, the alteration in muscles architecture was relatively limited in ATR patients with important functional deficits (9), pointing at the possible association between architectural compensatory changes and functional/clinical outcome. The differences between this study and others (9, 10) in the ratio of tendon/muscle length changes is worth noting.

Further studies should investigate the ratio of tendon to muscle length changes, as a potential predictor for functional deficit and as a benchmark indicator for (revision) surgery and rehabilitation.

4.7 Conclusion

Overall, the evolution of tendon healing after rupture and repair seems to start with an initial remodelling of sarcomeres in series due to the muscle slack caused by an elongated tendon. Changes in tendon stiffness and muscle architecture after rupture and repair are in theory capable to fully compensate tendon lengthening in the GM muscle in terms of resetting muscle fascicles to their optimal length for force production. This adaptation in the GM muscle and presumably the entire triceps surae comes at the cost of a reduced range of motion for active force generation. We contend that this effect largely explains the great force deficit seen in the investigated ATR patients.

Acknowledgement

Conflicts of interest

1. The authors declare that they have no conflict of interest.
2. The results of the study do not constitute endorsement by ACSM and are presented clearly, honestly, and without fabrication, falsification, or inappropriate data manipulation.
3. This research received no specific grant from any funding agency in the public, commercial, or non-profit sectors.

Ethics approval

This study was performed in line with the principles of the Declaration of Helsinki. Ethics approval was granted by the *institutional review board* of the German Sport University Cologne (10.01.2013).

Consent to participate

Informed consent was obtained from all individual participants included in the study.

Availability of data and material

The datasets generated and analyzed during the current study are available from the corresponding author on reasonable request.

Authors' contributions

BS, GPB and KA conceptualized research. BS, OS, FG, GL, GPB and KA designed research. BS acquired data. BS, FG and KA analyzed data. BS, OS and KA interpreted data. BS, OS and KA drafted manuscript. BS, OS, FG, GL, GPB and KA revised manuscript. All authors approved final manuscript.

References

1. Järvinen TA, Kannus P, Maffulli N, Khan KM. Achilles tendon disorders: etiology and epidemiology. Foot Ankle Clin. 2005;10(2):255–66.

2. Brumann M, Baumbach SF, Mutschler W, Polzer H. Accelerated rehabilitation following Achilles tendon repair after acute rupture - Development of an evidence-based treatment protocol. Injury. 2014;45(11):1782–90.

3. Maffulli N, Tallon C, Wong J, Peng Lim K, Bleakney R. No adverse effect of early weight bearing following open repair of acute tears of the Achilles tendon. The Journal of sports medicine and physical fitness. 2003;43(3):367–79.

4. Kangas J, Pajala A, Siira P, Hamalainen M, Leppilahti J. Early functional treatment versus early immobilization in tension of the musculotendinous unit after Achilles rupture repair: a prospective, randomized, clinical study. J Trauma. 2003;54(6):1171-80; discussion 80-1.

5. Moller M, Kalebo P, Tidebrant G, Movin T, Karlsson J. The ultrasonographic appearance of the ruptured Achilles tendon during healing: a longitudinal evaluation of surgical and nonsurgical treatment, with comparisons to MRI appearance. Knee surgery, sports traumatology, arthroscopy : official journal of the ESSKA. 2002;10(1):49–56.

6. Schepull T, Aspenberg P. Early controlled tension improves the material properties of healing human achilles tendons after ruptures: a randomized trial. The American journal of sports medicine. 2013;41(11):2550–7.

7. Horstmann T, Lukas C, Merk J, Brauner T, Mündermann A. Deficits 10-years after achilles tendon repair. International journal of sports medicine. 2012;33(6):474–9.

8. Silbernagel KG, Steele R, Manal K. Deficits in Heel-Rise Height and Achilles Tendon Elongation Occur in Patients Recovering From an Achilles Tendon Rupture. The American journal of sports medicine. 2012;40(7):1564-71.

9. Svensson RB, Couppé C, Agergaard A-S, et al. Persistent functional loss following ruptured Achilles tendon is associated with reduced gastrocnemius muscle fascicle length, elongated gastrocnemius and soleus tendon, and reduced muscle cross‐sectional area. Transl Sports Med 2019;2(6):316-24.

10. Peng WC, Chao YH, Fu ASN, et al. Muscular Morphomechanical Characteristics After an Achilles Repair. Foot Ankle Int. 2019;40(5):568-77.

11. Baxter JR, Hullfish TJ, Chao W. Functional deficits may be explained by plantarflexor remodeling following Achilles tendon rupture repair: Preliminary findings. J Biomech. 2018;79:238-42.

12. Schepull T, Kvist J, Aspenberg P. Early E-modulus of healing Achilles tendons correlates with late function: similar results with or without surgery. Scandinavian journal of medicine & science in sports. 2012;22(1):18–23.

13. Wang H-K, Chiang H, Chen W-S, Shih TT, Huang Y-C, Jiang C-C. Early neuromechanical outcomes of the triceps surae muscle-tendon after an Achilles' tendon repair. Archives of physical medicine and rehabilitation. 2013;94(8):1590–8.

14. Palmes D, Spiegel HU, Schneider TO, et al. Achilles tendon healing: long-term biomechanical effects of postoperative mobilization and immobilization in a new mouse model. J Orthop Res. 2002;20(5):939–46.

15. Bruns J, Kampen J, Kahrs J, Plitz W. Achilles tendon rupture: experimental results on spontaneous repair in a sheep-model. Knee Surg Sports Traumatol Arthrosc. 2000;8(6):364–9.

16. Schepull T, Kvist J, Andersson C, Aspenberg P. Mechanical properties during healing of Achilles tendon ruptures to predict final outcome: a pilot Roentgen stereophotogrammetric analysis in 10 patients. BMC musculoskeletal disorders. 2007;8:116.

17. Agres AN, Duda GN, Gehlen TJ, Arampatzis A, Taylor WR, Manegold S. Increased unilateral tendon stiffness and its effect on gait 2-6 years after Achilles tendon rupture. Scandinavian journal of medicine & science in sports. 2015;25(6):860-7.

18. Hullfish TJ, O'Connor KM, Baxter JR. Gastrocnemius fascicles are shorter and more pennate throughout the first month following acute Achilles tendon rupture. PeerJ. 2019;7:e6788.

19. Lichtwark GA, Wilson AM. Optimal muscle fascicle length and tendon stiffness for maximising gastrocnemius efficiency during human walking and running. Journal of theoretical biology. 2008;252(4):662–73.

20. Roberts TJ, Azizi E. Flexible mechanisms: the diverse roles of biological springs in vertebrate movement. The Journal of experimental biology. 2011;214(Pt 3):353–61.

21. Bressel E, McNair PJ. Biomechanical behavior of the plantar flexor muscle-tendon unit after an Achilles tendon rupture. The American journal of sports medicine. 2001;29(3):321–6.

22. Faul F, Erdfelder E, Lang AG, Buchner A. G*Power 3: a flexible statistical power analysis program for the social, behavioral, and biomedical sciences. Behav Res Methods. 2007;39(2):175-91.

23. Mullaney MJ, McHugh MP, Tyler TF, Nicholas SJ, Lee SJ. Weakness in end-range plantar flexion after Achilles tendon repair. Am J Sports Med. 2006;34(7):1120–5.

24. Thomas S, Reading J, Shephard RJ. Revision of the Physical Activity Readiness Questionnaire (PAR-Q). Can J Sport Sci. 1992;17(4):338-45.

25. Stenroth L, Peltonen J, Cronin NJ, Sipilä S, Finni T. Age-related differences in Achilles tendon properties and triceps surae muscle architecture in vivo. Journal of applied physiology (Bethesda, Md : 1985). 2012;113(10):1537–44.

26. Barfod KW, Riecke AF, Boesen A, et al. Validity and reliability of an ultrasound measurement of the free length of the Achilles tendon. Dan Med J. 2018;65(3).

27. Geremia JM, Baroni BM, Bini RR, et al. Triceps Surae Muscle Architecture Adaptations to Eccentric Training. Front Physiol. 2019;10:1456.

28. Stenroth L, Sillanpaa E, McPhee JS, et al. Plantarflexor Muscle-Tendon Properties are Associated With Mobility in Healthy Older Adults. J Gerontol A Biol Sci Med Sci. 2015;70(8):996-1002.

29. Seynnes OR, Bojsen-Moller J, Albracht K, et al. Ultrasound-based testing of tendon mechanical properties: a critical evaluation. J Appl Physiol (1985). 2015;118(2):133-41.

30. Mademli L, Arampatzis A, Morey-Klapsing G, Brüggemann G-P. Effect of ankle joint position and electrode placement on the estimation of the antagonistic moment during maximal plantarflexion. Journal of electromyography and kinesiology : official journal of the International Society of Electrophysiological Kinesiology. 2004;14(5):591–7.

31. An KN, Takahashi K, Harrigan TP, Chao EY. Determination of muscle orientations and moment arms. Journal of biomechanical engineering. 1984;106(3):280–2.

32. Maganaris CN, Baltzopoulos V, Sargeant AJ. In vivo measurement-based estimations of the human Achilles tendon moment arm. European journal of applied physiology. 2000;83(4 -5):363–9.

33. Kösters A, Wiesinger HP, Bojsen-Møller J, Müller E, Seynnes OR. Influence of loading rate on patellar tendon mechanical properties in vivo. Clinical biomechanics (Bristol, Avon). 2014;29(3):323–9.

34. Stosic J, Finni T. Gastrocnemius tendon length and strain are different when assessed using straight or curved tendon model. European journal of applied physiology. 2011;111(12):3151–4.

35. Zange J, Schopen K, Albracht K, et al. Using the Hephaistos orthotic device to study countermeasure effectiveness of neuromuscular electrical stimulation and dietary lupin protein supplementation, a randomised controlled trial. PLoS One [Internet]. 2017 PMC5313207]; 12(2). Available from: https://www.ncbi.nlm.nih.gov/pubmed/28207840. doi: 10.1371/journal.pone.0171562.

36. Muramatsu T, Muraoka T, Takeshita D, Kawakami Y, Hirano Y, Fukunaga T. Mechanical properties of tendon and aponeurosis of human gastrocnemius muscle in vivo. Journal of applied physiology (Bethesda, Md : 1985). 2001;90(5):1671–8.

37. Magnusson SP, Aagaard P, Dyhre-Poulsen P, Kjaer M. Load-displacement properties of the human triceps surae aponeurosis in vivo. J Physiol. 2001;531(Pt 1):277-88.

38. Delp SL, Anderson FC, Arnold AS, et al. OpenSim: open-source software to create and analyze dynamic simulations of movement. IEEE Trans Biomed Eng. 2007;54(11):1940-50.

39. Seth A, Hicks JL, Uchida TK, et al. OpenSim: Simulating musculoskeletal dynamics and neuromuscular control to study human and animal movement. PLoS Comput Biol [Internet]. 2018 Jul PMC6061994]; 14(7). Available from: https://www.ncbi.nlm.nih.gov/pubmed/30048444. doi: 10.1371/journal.pcbi.1006223.

40. Millard M, Uchida T, Seth A, Delp SL. Flexing computational muscle: modeling and simulation of musculotendon dynamics. J Biomech Eng. 2013;135(2):021005.

41. Ward SR, Eng CM, Smallwood LH, Lieber RL. Are current measurements of lower extremity muscle architecture accurate? Clin Orthop Relat Res. 2009;467(4):1074-82.

42. Tabary JC, Tabary C, Tardieu C, Tardieu G, Goldspink G. Physiological and structural changes in the cat's soleus muscle due to immobilization at different lengths by plaster casts. J Physiol. 1972;224(1):231-44.

43. Williams PE, Goldspink G. The effect of immobilization on the longitudinal growth of striated muscle fibres. Journal of Anatomy. 1973;116(Pt 1):45–55.

44. de Boer MD, Seynnes OR, di Prampero PE, et al. Effect of 5 weeks horizontal bed rest on human muscle thickness and architecture of weight bearing and non-weight bearing muscles. Eur J Appl Physiol. 2008;104(2):401-7.

45. Reeves NJ, Maganaris CN, Ferretti G, Narici MV. Influence of simulated microgravity on human skeletal muscle architecture and function. J Gravit Physiol. 2002;9(1):P153-4.

46. Csapo R, Maganaris CN, Seynnes OR, Narici MV. On muscle, tendon and high heels. J Exp Biol. 2010;213(Pt 15):2582-8.

47. Delp SL, Zajac FE. Force- and moment-generating capacity of lower-extremity muscles before and after tendon lengthening. Clin Orthop Relat Res. 1992(284):247-59.

48. Maganaris CN, Baltzopoulos V, Tsaopoulos D. Muscle fibre length-to-moment arm ratios in the human lower limb determined in vivo. J Biomech. 2006;39(9):1663-8.

49. Heikkinen J, Lantto I, Piilonen J, et al. Tendon Length, Calf Muscle Atrophy, and Strength Deficit After Acute Achilles Tendon Rupture: Long-Term Follow-up of Patients in a Previous Study. J Bone Joint Surg Am. 2017;99(18):1509-15.

50. Hansen M, Koskinen SO, Petersen SG, et al. Ethinyl oestradiol administration in women suppresses synthesis of collagen in tendon in response to exercise. J Physiol. 2008;586(12):3005-16.

Supplemental Digital Content

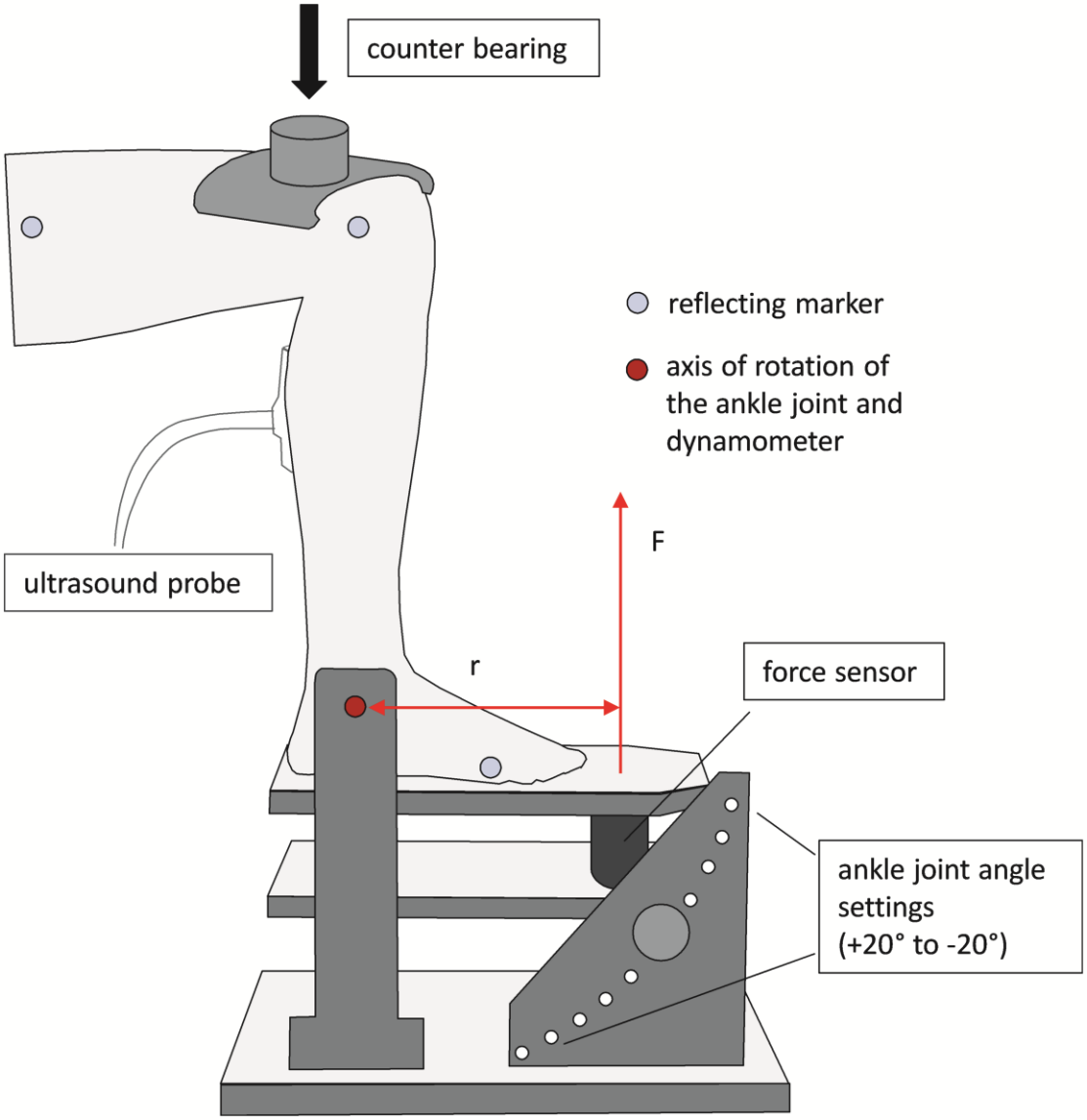

Supplemental Digital Content 1; Figure; Experimental set-up used to quantify the moment-angle relationship. Reflective markers defining thigh, shank and foot controlling knee and ankle angles. One dimensional strain gauge force sensor with the vertical force vector (F) and a fixed distance to center of rotation (r = 0.28m) for moment calculations. Ultrasound probe fixed on the gastrocnemius medialis muscle.

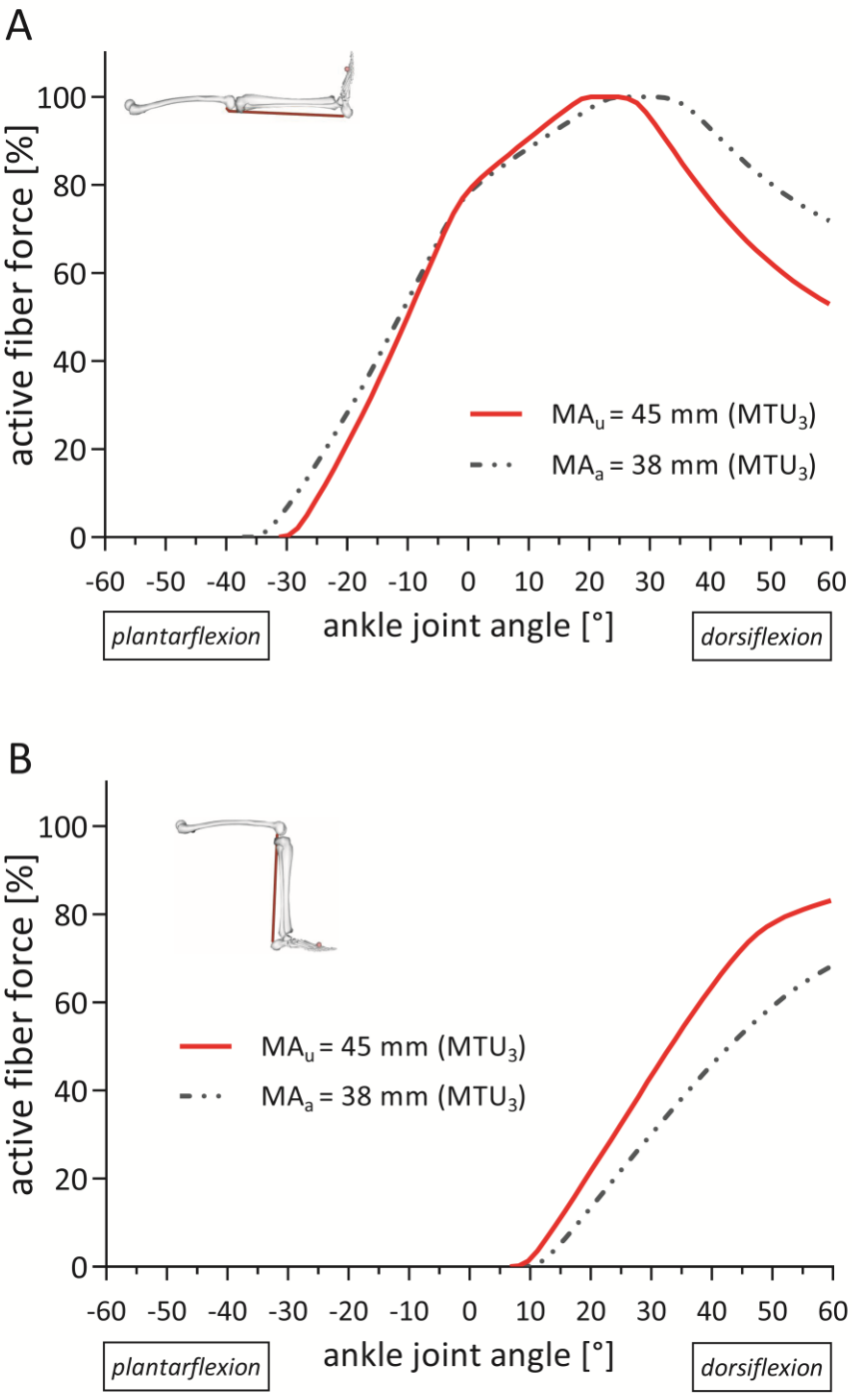

Supplemental Digital Content 2; Figure; Effect of Achilles tendon moment arm length on gastrocnemius medialis active fiber force generation in relation to ankle joint angle with an extended knee (A) and a 90° flexed knee (B). All curves represent the muscle-tendon unit of the affected side (MTU3) with varying moment arm length. MA_u: moment arm unaffected side, MA_a: moment arm affected side. MA_a was obtained by manipulating the calcaneal tendon insertion in the model.